Topological Surface States in Dense Solid Hydrogen

Ivan I. Naumov[1] and Russell J. Hemley[2,3]

[1]*Geophysical Laboratory, Carnegie Institution of Washington, Washington, D.C. 20015, USA*
[2]*Department of Civil and Environmental Engineering, The George Washington University, Washington, D.C. 20052, USA*
[3]*Lawrence Livermore National Laboratory, Livermore, California 94550, USA*

Metallization of dense hydrogen and associated possible high-temperature superconductivity represents one of the key problems of physics. Recent theoretical studies indicate that before becoming a good metal, compressed solid hydrogen passes through a semimetallic stage. We show that such semimetallic phases predicted to be the most stable at multimegabar ($\sim$300 GPa) pressures are not conventional semimetals: they exhibit topological metallic surface states inside the bulk "direct" gap in the two-dimensional surface Brillouin zone; that is, metallic surfaces may appear even when the bulk of the material remains insulating. Examples include hydrogen in the *Cmca*-12 and *Cmca*-4 structures; *Pbcn* hydrogen also has metallic surface states but they are of a nontopological nature. The results provide predictions for future measurements, including probes of possible surface superconductivity in dense hydrogen.

The behavior of hydrogen at high pressure is currently a subject of intense interest. At multimegabar pressures, the material is predicted to exhibit high-T_c superconductivity, superfluidity, and other unique metallic properties in its high-density solid and fluid phases [1–4]. Recent experimental and theoretical investigations suggest that at pressures beginning above 250 GPa solid hydrogen can transform into molecular *Cmca*-12 [5–11] and/or *Cmca*-4 [9–15] phases; the former can be insulating or semimetallic, whereas the latter is only semimetallic. We show that these phases are not conventional semimetals in that they have pronounced Shockley metallic surface states (SSs) of topological nature. These states are controlled by Zak's phase and form inside the "direct gap" between conduction and valence bands. They cover the whole two-dimensional surface Brillouin zone (BZ) in the case of *Cmca*-12 and only part of the zone for *Cmca*-4. Moreover, in *Cmca*-12 the SSs can coexist with the insulating bulk, whereas in *Cmca*-4 both surface and bulk states are always metallic. These results have important implications for characterizing semimetallic, metallic, and superconducting states of hydrogen being explored experimentally at multimegabar pressures.

In his seminal 1939 paper, Shockley showed how SSs appear in one-dimensional (1D) centrosymmetric crystals as the lattice parameter a decreases [16]. At some critical point a_c, the valence and conduction and valence bands cross, leaving two surface states within the bulk energy gap; at the a_c the latter closes and then immediately opens up, becoming "inverted." Much later, Zak realized that Shockley-type SSs have, in fact, a topological character [17]. He demonstrated that when the surface coincides with the symmetry centers, the existence or absence of the corresponding SSs is decided by the topology of the band below the gap. Of special interest in the general theory of

SSs is the case when the surface is taken between the atoms at the potential maxima, which is the situation that Shockley discussed in his pioneering work. In this case, speaking in more contemporary terms, the existence of SSs is related to the sum of all Zak's phases Z below the gap [18,19]. The SSs exist when the total phase is π and do not exist when it is 0. From the topological point of view, Shockley's critical parameter a_c is nothing but the point of topological transition at which the Zak's phase discontinuously changes from 0 to π.

Though Shockley and Zak considered only a simple 1D model, their results can be extended to systems of higher dimensions. As established recently, criteria for the existence of SSs are still applicable in centrosymmetric zero-gap semiconductors where the conduction and valence bands touch each other at points (2D *massless graphene-like* systems [20–22]) or along lines (3D *line-node topological semimetals* [23,24]). In such 2D and 3D materials, the existence of SSs with a particular momentum $\mathbf{k}_\parallel$ is controlled by the value of Zak's phase $Z(\mathbf{k}_\parallel)$ obtained by the integration across the BZ perpendicular to the edge or surface [20–24]. As in the 1D case, the SSs exist if $Z(\mathbf{k}_\parallel)$ is π (inverted band gaps) and do not if it is 0. For this, however, the phase Z becomes dependent on a new parameter $\mathbf{k}_\parallel$, which can be critical, similar to the lattice parameter a in the 1D case. The possible values of $Z(\mathbf{k}_\parallel)$, 0 or π, are completely defined by the positions of the band-contact points or lines. Thus, in graphene with zigzag edges, the SS states exist within a finite $\mathbf{k}_\parallel$-interval corresponding to the projection of the Dirac points $\mathbf{K}$ and $\mathbf{K}'$ on the $\mathbf{k}_\parallel$ axis, within this interval $Z(\mathbf{k}_\parallel) = \pi$ [20–22].

The line-node topological semimetals (LNTSs) can be viewed as 3D analogs of graphene. Instead of two separated Dirac points, they have an infinite number of effective

Dirac points merged together—band-contact lines lying at the Fermi level exactly (nodal lines) [23–25]. In LNTSs, the SSs appear within the whole $\mathbf{k}_\parallel$ area, where $Z(\mathbf{k}_\parallel) = \pi$; this area is limited by the projection of the nodal line (loop) onto the surface plane of interest [23–25]. The SSs are completely dispersionless and therefore characterized by an infinite density of states (DOS) at the Fermi level E_F [23–25]. This unphysical DOS reflects the fact that the LNTSs are actually idealized models where the band-contact line lies at the E_F [23]. In real materials, the probability that band-contact lines coincide with the E_F is vanishingly small [23]. Many systems, however, can be considered as "approximate" LNTSs where the contact lines have some dispersion and so do the SSs. Though SSs in "approximate" LNTSs acquire some dispersion, they still retain their topological nature and their existence can be predicted by the bulk Zak's phase [25,26]. Remarkably, the bulk Zak's phase is capable of capturing not only the difference between the surfaces of distinct orientations, but also the difference between the distinct terminations (if any) for a given orientation [21,22,24]. Such a nontrivial correspondence between the Zak's phases and surface terminations appears, owing to the convention that the surface is made by cutting a solid *between the primitive unit cells* [20–22] (we will refer to this as a *cutting rule*). This rule says that once the surface orientation and termination are specified they automatically specify the bulk primitive unit cell.

As a result of varying parameters in the crystal potential, the band crossing line (loop) can gradually disappear by shrinking to some point or "sinking" in the BZ boundary; this corresponds to a semimetallic-to-insulator transition. In the insulating state, the phase $Z(\mathbf{k}_\parallel)$ will become either 0 or π for all $\mathbf{k}_\parallel$ in the surface BZ [21,22]. The result depends on which part of the steplike distribution $Z(\mathbf{k}_\parallel)$ is extending. If $Z(\mathbf{k}_\parallel)$ is π everywhere, then the system should behave as a topological insulator: they are insulating in the bulk but necessarily have metallic surface states [21,22]. This is the case of *Cmca*-12 as we show below.

We begin with the *Cmca*-4 structure, which geometrically is close to hexagonal graphite: its primitive unit cell consists of four atoms and its layers are arranged in an *ABAB* sequence (Fig. 1). The calculated band structure of *Cmca*-4 hydrogen at 300 GPa shows that this system is in fact an approximate LNTS [Fig. 1(d)]. The valence and conduction bands intersect each other in a linear (Dirac-like) fashion for all the segments starting from the Y point. Since the Dirac-like points must lie on band contact lines normal to the corresponding segments [27], one can expect that they all belong to *one* band-crossing loop lying in the *xy* plane and encircling the point Y. Such a loop should induce SSs localized on a (001) surface. There are two possible terminations associated with this surface orientation. The first one breaks the long (weak) interlayer chemical bonds, whereas the second breaks the short (strong) intralayer bonds. According to the cutting rule, these two terminations correspond to two different primitive unit cells shown in Fig. 2 (yellow rectangles in
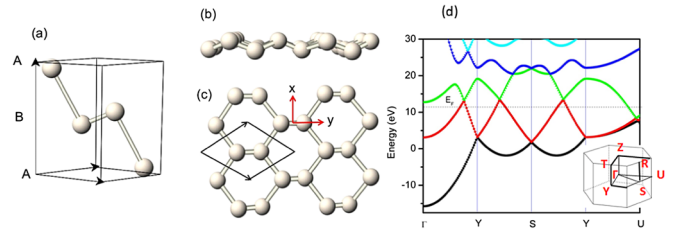

FIG. 1. Crystal and band structures of the hydrogen *Cmca*-4 phase. (a) Primitive unit cell, (b) side and (c) top of a single layer. (d) Segments that involve the Y point. The conduction and valence band intersections only approximately coincide with the Fermi level, indicating that the Fermi surface consists of small electron and hole pockets.

a and *b*). Hereafter, we call these terminations or unit cells "type *a*"and "type *b*."Since we treat the surfaces as boundary planes of the films repeated periodically in space at equal vacuum gaps, such films should be built from the complete bulk primitive unit cells as building blocks. Their thickness, therefore, can be specified by the number of bulk primitive cells stacked along the *z* axis (n). It is easy to see that an n-unit-cell thick film organized from type *a* unit cells contains n molecular layers A and n molecular layers B (see Figs. 1 and 2). At the same time, an n-unit-cell thick film organized from the type *b* unit cells contains $n-1$ molecular layers A, n molecular layers B (both inside the film), and, additionally, two atomic surface layers.

To check that the band-crossing loop and the corresponding SSs exist, we calculated the phases $Z(\mathbf{k}_\parallel)$ across the BZ in the z direction for both choices of the unit cell
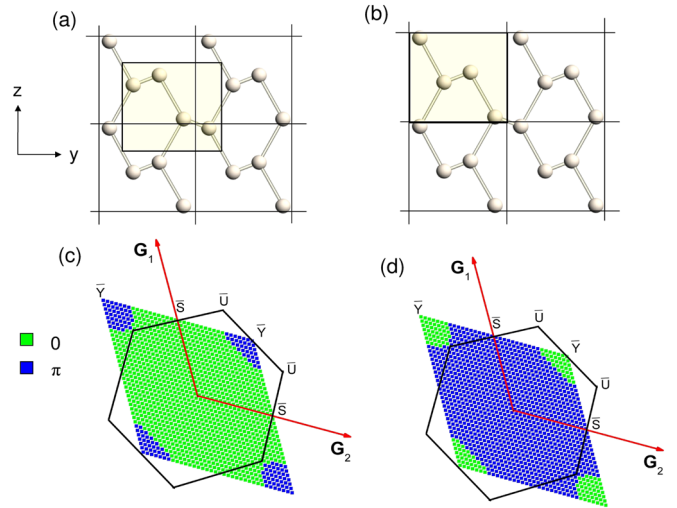

FIG. 2. (a),(b) Two choices of the primitive unit cell corresponding to two different surface terminations parallel to the *xy* plane, shown by yellow rectangles. For simplicity, we show the unit cells projected on the plane that contains all the 4 atoms shown in Fig. 1(a). (c) and (d) Zak's phase Z as a function of $\mathbf{k}_\parallel$ for the unit cells (a) and (b), respectively. The $\mathbf{k}_\parallel$ points are given on a 36×36 grid associated with the two in-plane reciprocal vectors, $\mathbf{G}_1$ and $\mathbf{G}_2$. The **k**-point labels correspond to those presented in Fig. 1(d). The phases 0, π are shown in green and blue, respectively.
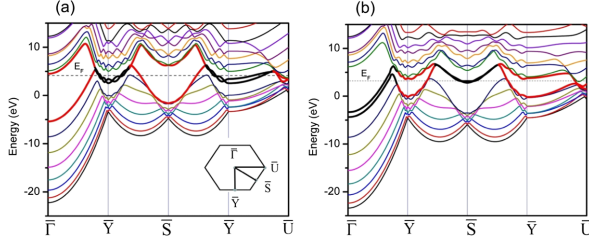
FIG. 3. Two-dimensional energy bands of hydrogen in a 4-unit-cell thick *Cmca*-4 structure. (a) Terminations that break long (weak) bonds on both sides of the film and (b) terminations that break short (strong) bonds. The surface bands are indicated by thick black curves that cross the E_F.

[Figs. 2(c) and 2(d)]. We treated our system as if it were an ideal LNTSs; *i.e.*, we assigned the number of "occupied" bands at each $\mathbf{k}_{\parallel}$ to be 2 (see the Supplemental Material [28]). For both cases the Zak's phase is quantized; *i.e.*, it takes only values 0 and π. For the type *a* case, the Zak's phase is 0 almost everywhere in the surface BZ except relatively small areas around the $\bar{Y}$ points [panel (c)]). In going from type *a* to *b*, all the $Z(\mathbf{k}_{\parallel})$ values shift by π, so that all the 0 phases become π and vice versa. These results suggest that in the type *a* case the SSs will cover a relatively small ellipselike area around the $\bar{Y}$ point, with the major radii almost reaching the $\bar{U}$ points, whereas in the type *b* case − a significant part of the surface BZ centered at $\bar{\Gamma}$.

Direct calculations of surface electronic structure for the 4-unit-cell thick films of H show that this is indeed the case (Fig. 3); the calculations for thicker films lead only to slightly different quantitative results. The surface bands obtained can be identified, indicated by thick black curves that cross the E_F. For type *a*, they appear around the $\bar{Y}$

point, in agreement with Fig. 2(c). In contrast, for type *b* they are realized everywhere in the surface BZ, but not in the vicinity of the $\bar{Y}$ point, again in accordance with the Zak's phase calculations. We thus see that the stronger the broken bonds, the larger is the **k** area covered by the corresponding SSs; this allows one to interpret the SSs as dangling bond surface states. Notably, upon moving away from their "natural habitats," the SSs gradually *turn* into bulk states, as shown by the thick red curves in Fig. 3. This reflects their topological nature and intimate relationship to the bulk electronic structure.

Figure 3 shows the SSs always appear in pairs, almost in the middle of the corresponding band gaps. One surface band falls out of the allowed bulk *valence* band and the other from the allowed *conduction* bulk band. Because of the presence of inversion symmetry, they are either symmetric or antisymmetric with respect to the operation $\mathbf{r} \to -\mathbf{r}$. They do not coincide in energy because the opposite sides of the film still "feel" each other. However, they become exactly degenerate as the film becomes infinitely thick. It is straightforward to prove using Shockley's arguments [16] that the SSs must be *metallic*. Indeed, in a *Cmca*-4 (001) hydrogen film there is *one more* band in the lowest, valence part of the spectrum relative to the similar effective bulk system. Therefore, this additional (surface) band must be partially occupied with electrons.

The charge distributions of the lower SS at different high-symmetry points in the $x = 0$ plane are given in Fig. 4. One can see that in the case of the type *a* termination, the density is mainly localized in the first and third surface layers, whereas for type *b* termination it is in the two upper atomic layers [Figs. 4(a), 4(b)]. Further, it easy to see that the charge on the opposite surfaces is
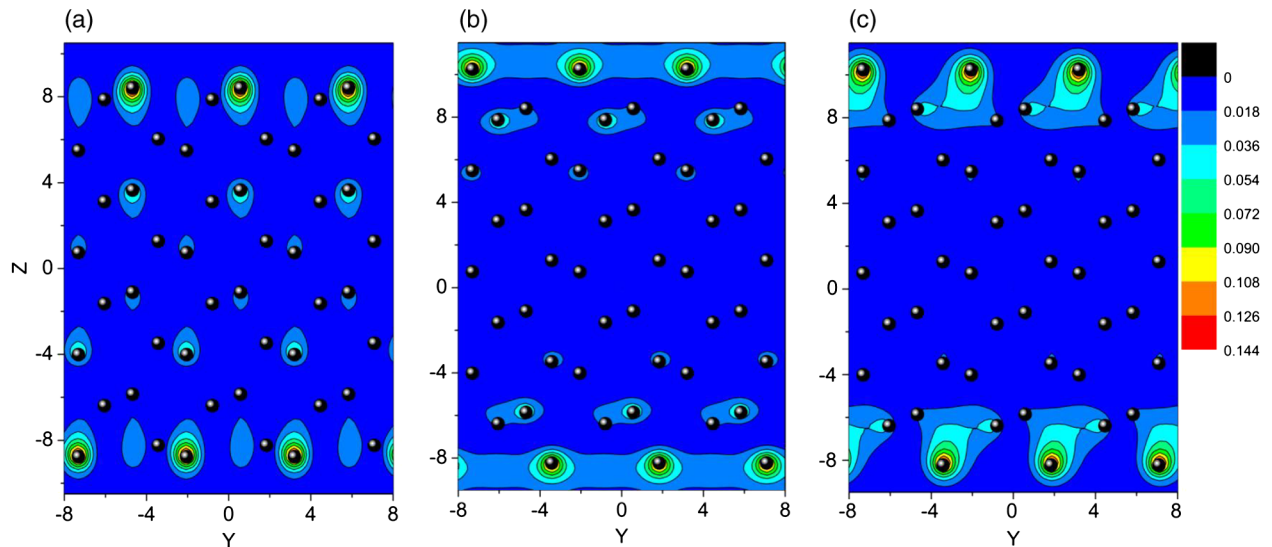

FIG. 4. The charge density of the lower (out of 2) surface state at different high-symmetry points in the surface BZ and different types of terminations, for 4-unit-cell-thick films in the $x = 0$ plane. The position of atoms along the z and y axes are given in Bohrs. (a) At the $\bar{Y}$ point for the *type a* termination. (b) and (c) at the $\bar{\Gamma}$ and $\bar{S}$ points, respectively, for the *type b* termination. Full black circles indicate the atomic positions. The surface atoms correspond to the top and bottom layers along the z direction. Note that the $x = 0$ plane coincides with that shown in Figs. 2(a), (b).

located on the *different nonoverlapping sublattices*. All sublattices corresponding to one surface can be obtained from the sublattices corresponding to the opposite surface by the inversion symmetry ($\mathbf{r} \rightarrow -\mathbf{r}$). The metallization of the surface for type *b* termination seems natural: in this case the molecular (strong) bonds on the surface are broken. The situation, however, is not as trivial for case *a* termination, which preserves the "H_2 "molecular structure of the surface layer. Even in this case the electronic structure of the layer is *metallic* in character and the wave function is localized essentially on only one of the two H atoms [Fig. 4(a)].

We now proceed to the orthorhombic *Cmca*-12 phase, which shares with *Cmca*-4 the same space group but has a different number of atoms per primitive unit cell [12; Fig. 5(a)]. At 300 GPa, this phase is a semimetal where the indirect band gap is closed due to lowering of the conduction band at the Y point below the E_F [Fig. 5(b)]. In order to check the existence of SSs on the surfaces normal to the *x*, *y*, and *z*, we calculated Zak's phases along the shortest reciprocal lattice vectors $\mathbf{G}_1$, $\mathbf{G}_2$, and $\mathbf{G}_3$ using a conventional (nonprimitive) unit cell with 24 atoms. We treated the system as if it was a real dielectric by assigning the number of occupied bands to be 12 at each $\mathbf{k}_{\parallel}$. The phases were measured relative to their ionic [35] counterparts. We found them to be zero for all $\mathbf{k}_{\parallel}$ if they are integrated along the $\mathbf{G}_1$ (*x*) and $\mathbf{G}_2$ (*y*) directions. However, they are all π if integrated along the $\mathbf{G}_3$ (*z*) direction. This means that the localized SSs should form on both (001) surfaces of a
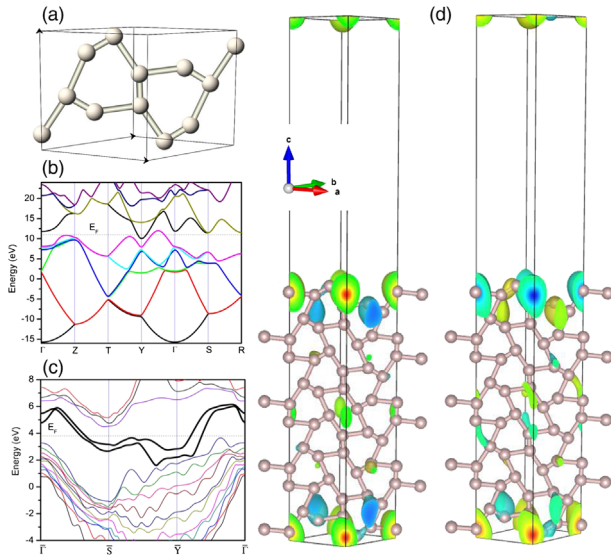

FIG. 5. Crystal and band structures of the *Cmca*-12 phase. (a) Primitive unit cell. (b) Bulk band structure at 300 GPa. (c) Band structure of a 4-unit-cell thick (001) film corresponding to the same pressure. The surface bands are indicated by thick black curves crossing the Fermi level. Their energies become equal to each other when the film thickness tends to infinity. (d) Isosurfaces (±1.75) of two Bloch functions at the $\bar{S}$ point— symmetric (right) and antisymmetric (left) with respect to the inversion center. The functions are shown in the used supercell consisting of atomic layers and vacuum gaps.

Cmca-12 slab provided that the latter is organized from the complete bulk unit cells [36]. The direct calculations of the band structure confirm that this is indeed the case [Fig. 5(c)]. As for *Cmca*-4, we can see that there are two surface states that cross the E_F. Now, however, they cover the whole surface BZ. Because of the presence of the center of symmetry, these states are either symmetric or antisymmetric with respect to the inversion center ($\mathbf{r} \rightarrow -\mathbf{r}$), as illustrated in Fig. 5(d) for the $\bar{S}$ point. Correspondingly, they become degenerate if the film is thick enough. It is important that the SSs appear even *before* the system becomes semimetallic in the bulk.

Experimentally, distinguishing between possible surface and bulk conductivities can be challenging, as is the case for topological insulators [28]. When the bulk is still insulating but the surface becomes metallic, the optical conductivity at frequencies of order <0.2 eV will be completely determined by surface states lying within the bulk energy gap [28]. In the Cmca-4 phase, bulk and surface conductivities always coexist, as mentioned above. For this structure, disentangling the surface and bulk contributions can be facilitated by specific behavior of the latter. It turns out that low-frequency bulk conductivity of *Cmca*-4 hydrogen parallels that of graphite because the two materials resemble each other both structurally and electronically [37–39]. Using the Kubo-Greenwood formula we found that like graphite, the zero-temperature conductivity per layer, σ^{2D}, of *Cmca*-4 hydrogen is very close to the universal value of $\pi e^2 / 2h$ predicted for monolayer graphene [40,41] (in our case $\sigma^{2D} \sim 1.07 \times \pi e^2 / 2h$). Moreover, the bulk optical conductivity remains close to this universal value at finite temperatures in the range of photon energies between 0.2 and 1.0 eV, as in graphite. This implies that any noticeable change in the total conductivity within this range should be solely due to the surface contribution. We expect that this contribution is higher in amplitude due to elevated DOS at the E_F in the surface layer. The local DOS at the E_F significantly increases upon formation of the (001) surfaces—by a factor of 3 and 10 for type *a* and *b* terminations, respectively (Fig. S3). The local DOS for the atoms belonging to the central layer is typical for bulk *Cmca*-4 hydrogen, where the E_F is in the minimum of DOS. The increase in this quantity as one approaches the surface of the type *b*, for example, is explained by the surface states around the $\bar{Y}$ point [Fig. 3(b)].

Different high-pressure structures of hydrogen are prone to have metallic SSs, but the existence of such SSs cannot always be predicted from the corresponding bulk band structures. For example, the *Pbcn* structure that has been used to interpret experimental data for the phase IV [42,43] exhibits pronounced "nontopological" SSs despite the absence of the bulk-surface correspondence discussed above [28]. We believe that similar effects should take place even in fluid molecular hydrogen undergoing a pressure-induced metallization process via pseudogap closure. In this case, dangling bonds related to those identified here at the surface lead to the additional localized states in

the pseudogap [44], thereby increasing the DOS at E_F. The system can reach a point at which states at E_F are no longer localized, and these critical metallic states are likely to be confined to the surface rather than to be bulk. Topological SSs similar to those discussed here for hydrogen can also form in some simple sp metals. For example, the pronounced Shockley states found earlier in Be on its (0001) surface around the $\bar{\Gamma}$ point [45] could have been also predicted from Zak's phase calculations. Because of their topological nature, these states are relatively flat; according to Ref. [46] the local DOS at the E_F is four times larger than in the bulk. It has been suggested that such a situation can trigger an unusual form of surface superconductivity with very high T_c [46]. By analogy, one can expect the existence of such surface superconductivity in compressed hydrogen.

[1] V. L. Ginzburg, Phys. Usp. **42**, 353 (1999).
[2] N. W. Ashcroft, Phys. Rev. Lett. **21**, 1748 (1968).
[3] H. K. Mao and R. J. Hemley, Rev. Mod. Phys. **66**, 671 (1994).
[4] J. M. McMahon, M. A. Morales, C. Pierleoni, and D. M. Ceperley, Rev. Mod. Phys. **84**, 1607 (2012).
[5] M. I. Eremets and I. A. Troyan, Nat. Mater. **10**, 927 (2011).
[6] R. P. Dias, O. Noked, and I. F. Silvera, arXiv:1603.02162v2.
[7] C. J. Pickard and R. J. Needs, Nat. Phys. **3**, 473 (2007).
[8] S. Lebègue, C. M. Araujo, D. Y. Kim, M. Ramzan, H. K. Mao, and R. Ahuja, Proc. Natl. Acad. Sci. U.S.A. **109**, 9766 (2012).
[9] C. J. Pickard, M. Martinez-Canales, and R. J. Needs, Phys. Rev. B **85**, 214114 (2012); **86**, 059902(E) (2012).
[10] S. Azadi, W. M. C. Foulkes, and T. D. Kühne, New J. Phys. **15**, 113005 (2013).
[11] S. Azadi, B. Monserrat, W. M. C. Foulkes, and R. J. Needs, Phys. Rev. Lett. **112**, 165501 (2014).
[12] K. A. Johnson and N. W. Ashcroft, Nature (London) **403**, 632 (2000).
[13] J. M. McMahon and D. M. Ceperley, Phys. Rev. Lett. **106**, 165302 (2011).
[14] H. Liu, L. Zhu, W. Cui, and Y. Ma, J. Chem. Phys. **137**, 074501 (2012).
[15] A. F. Goncharov, J. S. Tse, H. Wang, J. Yang, V. V. Struzhkin, R. T. Howie, and E. Gregoryanz, Phys. Rev. B **87**, 024101 (2013).
[16] W. Shockley, Phys. Rev. **56**, 317 (1939).
[17] J. Zak, Phys. Rev. B **32**, 2218 (1985).
[18] M. Xiao, Z. Q. Zhang, and C. T. Chan, Phys. Rev. X **4**, 021017 (2014).
[19] M. Xiao, G. Ma, Z. Yang, P. Sheng, Z. Q. Zhang, and C. T. Chan, Nat. Phys. **11**, 240 (2015).
[20] S. Ryu and Y. Hatsugai, Phys. Rev. Lett. **89**, 077002 (2002).
[21] P. Delplace, D. Ullmo, and G. Montambaux, Phys. Rev. B **84**, 195452 (2011).
[22] T. Kariyado and Y. Hatsugai, Phys. Rev. B **90**, 085132 (2014).
[23] A. A. Burkov, M. D. Hook, and L. Balents, Phys. Rev. B **84**, 235126 (2011).
[24] R. Takahashi and S. Murakami, Phys. Rev. B **88**, 235303 (2013).
[25] T. T. Heikkilä, N. B. Kopnin, and G. E. Volovik, JETP Lett. **94**, 233 (2011).
[26] R. Xiao, F. Tasnádi, K. Koepernik, J. W. F. Venderbos, M. Richter, and M. Taut, Phys. Rev. B **84**, 165404 (2011).
[27] C. Herring, Phys. Rev. **52**, 365 (1937).
[28] See Supplemental Material at http://link.aps.org/supplemental/10.1103/PhysRevLett.117.206403, which contains Refs. [29–34], details of calculations and additional discussion.
[29] X. Gonze et al., Comput. Phys. Commun. **180**, 2582 (2009).
[30] H. J. Monkhorst and J. D. Pack, Phys. Rev. B **13**, 5188 (1976).
[31] R. Resta and D. Vanderbilt, *Physics of Ferroelectrics: A Modern Perspective, Topics in Applied Physics*, edited by C. H. Ahn, K. M. Rabe, and J.-M. Triscone (Springer, Berlin, 2007), Vol. 105, p. 31.
[32] C. Durand, X.-G. Zhang, S. M. Hus, C. Ma, M. A. McGuire, Y. Xu, H. Cao, I. Miotkowski, Y. P. Chen, and A.-P. Li, Nano Lett. **16**, 2213 (2016).
[33] K. Hoefer, C. Becker, D. Rata, J. Swanson, P. Thalmeier, and L. H. Tjeng, Proc. Natl. Acad. Sci. U.S.A. **111**, 14979 (2014).
[34] L. L. Li, W. Xu, and F. M. Peeters, J. Appl. Phys. **117**, 175305 (2015).
[35] R. D. King-Smith and D. Vanderbilt, Phys. Rev. B **47**, 1651 (1993).
[36] The "topological" character of the *Cmca*-12 phase can be easily checked. By increasing the lattice parameter along the z axis and keeping all the other structural parameters the same, one can induce a band contact line in the xy plane around the Y point similar to that in *Cmca*-4.
[37] I. I. Naumov, R. E. Cohen, and R. J. Hemley, Phys. Rev. B **88**, 045125 (2013).
[38] R. E. Cohen, I. I. Naumov, and R. J. Hemley, Proc. Natl. Acad. Sci. U.S.A. **110**, 13757 (2013).
[39] I. I. Naumov and R. J. Hemley, Acc. Chem. Res. **47**, 3551 (2014).
[40] A. B. Kuzmenko, E. van Heumen, F. Carbone, and D. van der Marel, Phys. Rev. Lett. **100**, 117401 (2008).
[41] K. F. Mak, L. Ju, F. Wang, and T. F. Heinz, Solid State Commun. **152**, 1341 (2012).
[42] R. T. Howie, C. L. Guillaume, T. Scheler, A. F. Goncharov, and E. Gregoryanz, Phys. Rev. Lett. **108**, 125501 (2012).
[43] C. S. Zha, Z. Liu, and R. J. Hemley, Phys. Rev. Lett. **108**, 146402 (2012).
[44] N. F. Mott, *Metal-Insulator Transitions* (Taylor & Francis London, New York, Philadelphia, 1990), p. 286.
[45] E. V. Chulkov, V. M. Silkin, and E. N. Shirykalov, Surf. Sci. **188**, 287 (1987).
[46] T. Balasubramanian, E. Jensen, X. L. Wu, and S. L. Hulbert, Phys. Rev. B **57**, R6866 (1998).